

Superconductor to weak-insulator transitions in disordered Tantalum Nitride films

Nicholas P. Breznay,¹ Mihir Tendulkar,¹ Li Zhang,¹ Sang-Chul Lee,² and Aharon Kapitulnik^{1,3}

¹*Department of Applied Physics, Stanford University, Stanford, CA**

²*Department of Materials Science and Engineering, Stanford University, Stanford, CA*

³*Department of Physics, Stanford University, Stanford, CA*

(Dated: March 5, 2022)

We study the two-dimensional superconductor-insulator transition (SIT) in thin films of tantalum nitride. At zero magnetic field, films can be disorder-tuned across the SIT by adjusting thickness and film stoichiometry; insulating films exhibit classical hopping transport. Superconducting films exhibit a magnetic field-tuned SIT, whose insulating ground state at high field appears to be a quantum-corrected metal. Scaling behavior at the field-tuned SIT shows classical percolation critical exponents $z\nu \approx 1.3$, with a corresponding critical field $H_c \ll H_{c2}$. The Hall effect shows a crossing point near H_c , but with a non-universal critical value ρ_{xy}^c comparable to the normal state Hall resistivity. We propose that high-carrier density metals will always exhibit this pattern of behavior at the boundary between superconducting and (trivially) insulating ground states.

I. INTRODUCTION

The common approach to understanding disordered two dimensional electron systems like amorphous thin films is to assume that as the temperature T approaches zero, they can be either insulating (I) or superconducting (S). Driving them across the S-I phase boundary with disorder or magnetic field was predicted to realize a quantum phase transition — the superconductor-insulator transition (SIT)¹. Early experimental and theoretical studies of the SIT addressed the nature of an amplitude or phase dominated transition — see Ref. 2 for reviews — while more recently, evidence for unconventional ground states proximal to the SIT has emerged. These include metallic phases^{3–5} precluded by the scaling theory of localization⁶ as well as a Bosonic “Cooper-pair insulator” ground state^{7,8}. Further, the nature of the transition itself shows different regimes of behavior with changes in the degree of material disorder.

The limit of strong disorder⁹ reveals a direct, self-dual superconductor to Bosonic-insulator transition^{10,11}. When disorder is weak and the normal state shows quantum-corrected metallic behavior, the field-tuned SIT shows distinct critical behavior from the strong-disorder case^{3,12} that is interrupted as $T \rightarrow 0$ by a still unexplained and controversial metallic state. Observed in a range of amorphous^{13,14} and crystalline^{15,16} materials, a theoretical consensus has yet to emerge to explain this metallic behavior^{17–21}; recent experiments confirm it to be of “failed” superconducting character²². What separates the strong- and weak-disorder behavior regimes remains unclear, and may be due to the inhomogeneous and/or granular nature of the disorder, properties of the normal state, or properties of the proximal superconductivity. As yet there are few systems where careful control of the materials system can be combined with studies across both the disorder- and field-tuned SIT.

The field- and disorder-driven suppression of superconductivity has been studied in 2D intermetallic films, such as NbSi, TiN, NbN, MoGe, and amorphous indium oxide

(InO_x)^{12,23–26}. Notably, TiN shows what appears to be a direct field-tuned SIT and unexpected metallic saturation in the high-field insulating state²⁷, while both NbSi and NbN can be tuned via thickness or composition across the disorder-driven SIT.^{28,29} Tantalum thin films show a metal intervening in the SIT as a function of field and disorder. Qin et al.¹⁴ studied field-tuned transitions of several nm thick Ta films, observing hysteretic I-V characteristics and metallic saturation of the resistance at low temperature similar to that observed in MoGe³ and arguing that it is not a simple heating effect³⁰. In subsequent work³¹, I-V characteristics were used to identify superconducting, metallic, and insulating behavior, while very recent studies have examined critical scaling in both the superconducting and metallic phases³². In pure Ta there is no direct SIT; a metallic phase appears to intervene at all disorder strengths accessible by tuning the film thickness. These differences between materials families raise a central question: how does the SIT evolve under alternative disorder tuning parameters.

Here we study a strongly spin-orbit coupled binary metal nitride system, amorphous tantalum nitride (α -Ta_xN_{1-x}), where the disorder can be controlled by tuning film thickness and composition. The most disordered films show hopping transport at low temperatures, with no evidence for superconductivity. Weakly superconducting films can be driven into an insulating state beyond an applied magnetic field H_c , and show a temperature-independent crossing point at H_c and finite-size scaling in ρ_{xx} that is the hallmark of the SIT. We also report similar crossing and weak scaling behavior in the Hall effect ρ_{xy} , previously observed only in InO_x³³, with a non-universal value for the critical Hall resistivity ρ_{xy}^c . Along with evidence for unusual metallic behavior on the insulating side of the field-tuned SIT, similarities with other materials point towards a universal superconductor-weak insulator transition (SWIT). Finally, as normal-state Hall effect data indicate metallic carrier concentrations for all superconducting film ($n \sim 10^{23} \text{ cm}^{-3}$) comparable to MoGe, Ta, and other SWIT materials, we hypothesize that such large carrier densities preclude observation of a Bosonic

SIT.

This article is organized as follows: sample growth and characterization data are presented in Sec. II, while low-temperature transport data and the disorder-tuned SIT are described in Sec. III. The behavior in the vicinity of the field-tuned SIT is described in Sec. V, with scaling analyses considered in detail in Sec. VI. Section VII describes the Hall effect in the vicinity of the field-tuned SIT, where a crossing point and faint scaling appears above the critical field H_c . Finally, Sec. VIII summarizes the disorder and field-tuned SIT phenomenology in a -Ta N_x and discusses their implications.

II. FILM GROWTH AND CHARACTERIZATION

We study reactively sputtered a -Ta N_x films, most with thickness $d \sim 5 - 20$ nm, as described in part in previous work^{34,35}. Reactive sputtering with a tantalum target in a background Ar/ N_2 mixture is a common technique for growth of TaN films^{36–38}. In sputtered films, superconductivity with T_c between 5 and 10 K has been shown to be stable for a range of nitrogen stoichiometries³⁹; thick films can show T_c values as high as 10.9 K^{39–42}. Our films are grown using a commercial AJA reactive magnetron sputtering tool and pure Ta target in flowing Ar- N_2 gas. The Ar/N ratio controls the film Ta/N stoichiometry (and related film properties, such as the room temperature value of ρ_{xx})^{36–38}. Base pressure of the sputter deposition system was $\approx 10^{-8}$ torr. Films were co-deposited onto several substrate materials, including intrinsic Si, Si with SiO_2 and Si_3N_4 buffer layers, and glass; aside from few-percent quantitative differences in film properties (such as the room temperature resistivity ρ_{xx}) we found no sensitivity of film parameters to the choice of substrate. All substrates were Ar-ion plasma cleaned before sputtering. Pure Ta (and Ta-rich) films were also sputtered in identical conditions and comparable behavior to previous studies¹⁴; results from one Ta-rich film (N3) are included below for comparison.

Several parameters can be used to tune to the disorder in a -Ta N_x (as reflected in e.g. ρ_{xx} at room temperature), including thickness, N_2 partial pressure (and therefore stoichiometry x), and other synthesis conditions. Here we control the effective film disorder by changing the thickness and (for the $d \sim 5$ nm films) nitrogen stoichiometry. Table I shows the film growth and characterization parameters, including the stoichiometry x , thickness d , and electronic properties (discussed further below).

We characterize the film thickness, morphology, chemical composition, and homogeneity with a range of techniques. TEM measurements (Fig. 1) reveal the homogeneous and disordered a -Ta N_x film in sample N2 on a Si substrate; this film is 4 nm thick and approximately stoichiometric. The a -Ta N_x film cross section is enlarged in Fig. 1B; the scale bar in this panel is 4 nm. X-ray photoelectron spectroscopy (XPS) measurements confirm the

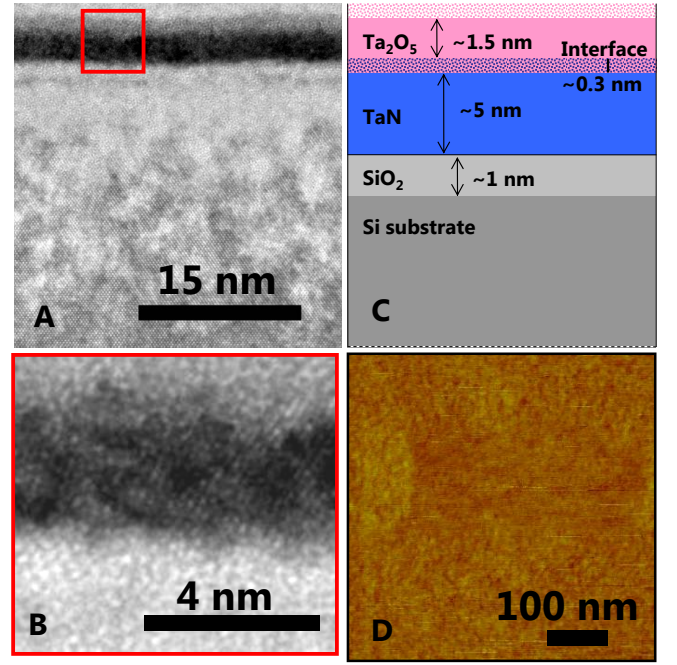


FIG. 1. (A) Cross-sectional TEM image of a -Ta N_x film on Si substrate, along with (B) inset showing the ~ 4 nm thick amorphous film. (C) Schematic diagram of the film composition and structure based on TEM and x-ray analyses. (D) AFM image with roughness of 0.2 nm; the full range of the color scale is 2 nm.

film stoichiometries, with an accuracy of $\approx 10\%$, shown in Tab. I; depth profiling uncovers a ~ 1 nm surface oxide layer on all films. A schematic of the film cross section including a the Si substrate, a -Ta N_x film, along with interfacial SiO_2 and TaO_x layers (with roughness ~ 0.5 nm) is shown in Fig. 1C. Scanning atomic-force microscopy measurements, shown in Fig. 1D for sample N2, show excellent homogeneity in the film thickness. The rms roughness is 0.1 nm (or 2% of the TaN layer thickness) over a $\sim 1\mu m^2$ region, with no evidence for granularity or inhomogeneity on this scale. (The full range of the color scale in Fig. 1D is 2 nm.) Scanning electron microscope imaging also showed no sign of inhomogeneity at the 10 nm length scale.

Figure 2A presents x-ray reflectivity data for two films (N2 and N3) and best-fit model curves (continuous lines). The nonlinear curve fitting analysis also yields film densities $\rho(TaN) \approx 15.9 \text{ g/cm}^3$, consistent with bulk values. Film phase and composition were also analyzed using x-ray diffraction, shown in Fig. 2B, which confirm the amorphous nature of the a -Ta N_x films studied here. Broad amorphous peaks at 36° , 42° , and 60° corresponding to the (111), (200), and (220) peaks of FCC δ -TaN are visible in the curve for the thickest (250 nm) sample N0. The curve for sample N1 (36 nm) barely shows the same FCC δ -TaN peaks, as well as peaks at 38° and 44° from orthorhombic Ta_2O_5 (often seen for sputtered Ta N_x films⁴³), again indicating the 1 nm of tantalum ox-

TABLE I. Disordered TaN_x film electronic and structural properties, including the thickness d , superconducting transition temperature T_c , longitudinal sheet resistivity ρ_{xx} , low-field Hall coefficient R_H , and carrier density n .

Sample Name	SC/Ins.	TaN_x stoichiometry x	d (nm)	T_c (K)	ρ_{xx} (300K) (Ω/\square)	R_H (Ω/T)	n (10^{22} cm^{-3})
N0	SC	1.0 ± 0.1	250	6.4	10.6	-	-
N1	SC	1.1	36	3.7	507	0.0022	7.9
N2	SC	1.0	4.0	2.8	828	0.014	11.1
N3	SC	0.1	4.9	0.5	526	0.029	4.4
N4	SC	1.1	5.9	0.7	1.3×10^3	0.011	9.6
N5	Ins.	1.2	5.3	-	8.0×10^3	-	-
N6	Ins.	1.4	4.9	-	13×10^3	-	-
N7	Ins.	1.6	5.2	-	1.4×10^6	-	-

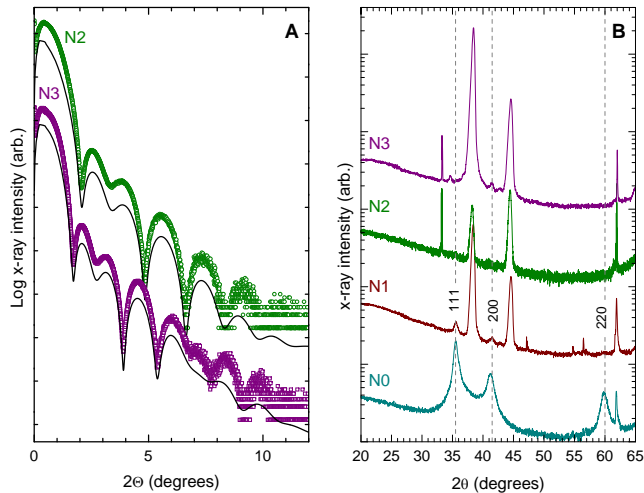


FIG. 2. (A) X-ray reflectivity scans for samples N2 and N3, along with fits (solid lines). (B) X-ray diffraction $\theta - 2\theta$ scan of samples N0-N3; curves have been vertically offset for clarity. Only sample N0 shows broad (111), (200), and (220) peaks associated with *fcc*- Ta_xN ; peaks visible for films N1-N3 are due to the substrate or surface TaO_x layer.

ide found previously. The most thin ($d \sim 4 - 5$ nm) films show additional sharp peaks from the Si substrate, but no sign of crystalline order from the *a*- TaN_x layer.

In summary, films studied here are amorphous, continuous, and homogeneously disordered. This is reflected in the electronic properties, which show disorder-limited length scales (such as the mean free path ℓ) much smaller than the film thickness.

III. EXPERIMENTAL DETAILS AND SUPERCONDUCTOR-INSULATOR TRANSITION

Films were patterned into Hall-bar geometry devices (see the inset of Fig. 3) and measured using standard low-frequency techniques; see Ref. 34 for additional experimental details. All applied magnetic fields H were perpendicular to the film plane. Care was taken to avoid

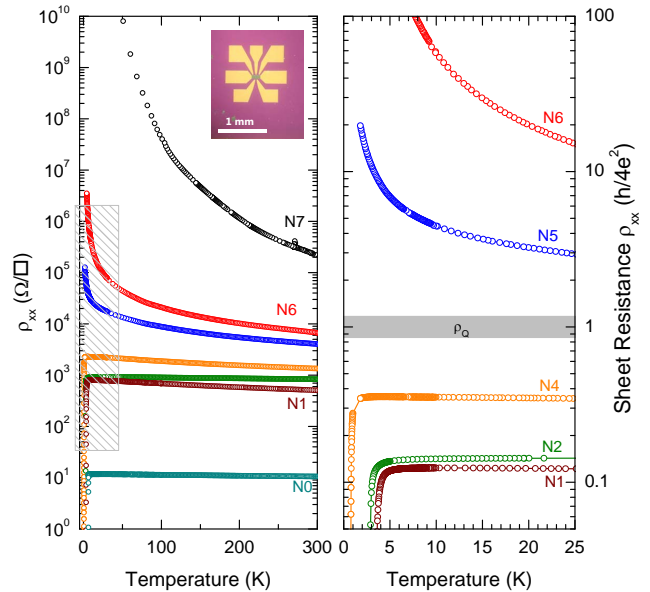


FIG. 3. Sheet resistance versus temperature for a series of disordered Tantalum Nitride films. Disorder increases with decreasing thickness or increasing the nitrogen concentration x in Ta_xN films. The hatched region at left is plotted in panel at right, where the horizontal gray bar indicates $\rho_Q = 6.45 \text{ k}\Omega$.

electron heating during measurements below 1 K and during magnetic field ramps; all ρ_{xx} and ρ_{xy} measurements were confirmed to be ohmic. Reported longitudinal resistivities ρ_{xx} and Hall resistivities ρ_{xy} are 2D (sheet) quantities, unless explicitly noted otherwise. Table I shows electrical transport data for the eight *a*- Ta_xN films discussed here, five superconducting (N0-N4) and three insulating (N5-N7). The T_c is determined where ρ_{xx} has fallen to 1% of the normal-state value, for consistency. Also shown are the 300 K ρ_{xx} , Hall coefficient R_H , and the carrier density n estimated using a single parabolic band model appropriate for these strongly disordered films.

Hall measurements show ρ_{xy} linear in field and generally n-type carrier densities $\sim 10^{23} \text{ cm}^{-3}$, reported in Tab. I. Previous studies observed a change from n- to p- carrier type at $x \sim 1.67$ ⁴⁴. Bulk film resistiv-

ities are as low as $\rho_{xx} \sim 1 \text{ m}\Omega\text{-cm}$, depending on the stoichiometry, again comparable to films on the boundary of the stoichiometry-tuned metal-insulator transition.⁴⁴ The mean free paths for superconducting films are $\ell \sim 0.1 \text{ nm}$, with $k_F\ell \sim 1.0 - 3.0$ where k_F is the Fermi wavevector. With the exception of the $d \sim 250 \text{ nm}$ thick sample N0, all films can be considered 2D in the context of superconductivity ($\xi < d$) and disorder-induced localization ($L_\phi < d$) effects^{34,35}.

Figure 3 shows the resistivity for all films as a function of temperature and illustrates the distinct superconducting and insulating ground states available to these materials as the disorder is changed. Similar behavior is observed in materials where the transition is tuned by thickness (such as in Bi^{45}) or otherwise controlling the disorder (e.g. TiN^5). The separatrix between superconducting and insulating curves is $\rho_Q = h/4e^2$, highlighted in the right panel of Fig. 3 that shows the low-temperature region near ρ_Q . The superconducting T_c of sputtered TaN films has been reported as high as $\sim 11 \text{ K}$ for thick films^{39–42}; the maximum T_c observed here is 6.9 K for thickest (250 nm) film studied, N0.

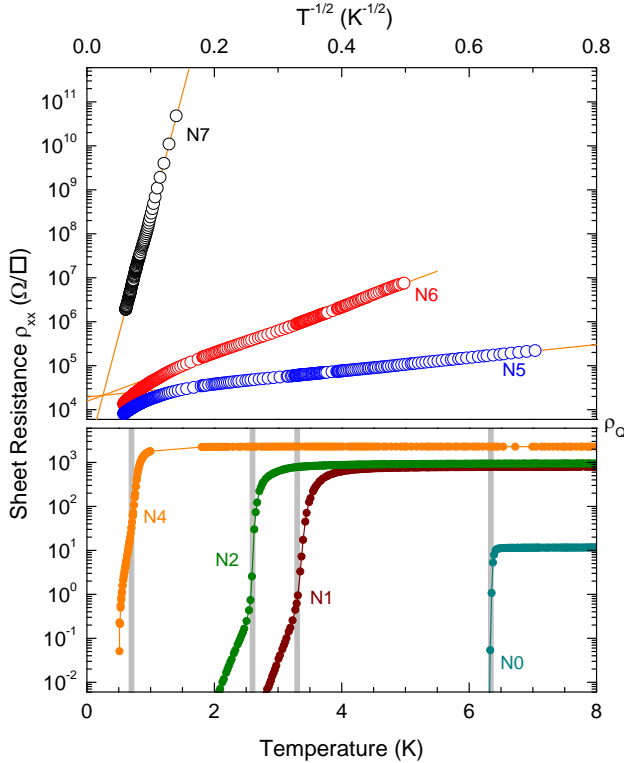


FIG. 4. Sheet resistance ρ_{xx} of insulating TaN_x films (upper panel) versus $T^{-1/2}$; the linear behavior is consistent with Efros-Shklovskii⁴⁶ hopping transport arising from a depletion of the electronic density of states due to coulomb interactions. Superconducting films (lower panel) show a crossover from 3D to 2D behavior, and finite size effects appearing as a tail below T_c (gray bars); lines are guides to the eye.

IV. ZERO FIELD GROUND STATES

Here we characterize the superconducting and insulating ground states of the $a\text{-TaN}_x$ films in the absence of an applied field, as the disorder is tuned via nitrogen stoichiometry. Beginning with the highest-disorder samples, Fig. 3 shows strong insulating behavior for samples N5–N7, with ρ_{xx} increasing exponentially with temperature. The upper panel of Fig. 4 shows $\rho_{xx}(T)$ plotted versus $T^{-1/2}$, along with straight-line fits of the Efros-Shklovskii form:

$$\rho_{xx}(T) = \rho_0 \exp \left[(T_0/T)^{1/2} \right] \quad (1)$$

where ρ_0 and T_0 are fitting parameters; the values for T_0 range from 50 K for sample N7 to 2 K for N5 as often observed in amorphous insulating materials.⁴⁷ The lowest measurement temperatures accessible for the insulating films are $\sim T_0$, hence we cannot conclusively establish the presence of a coulomb gap. However, both samples N6 and N7 are strongly localized insulators with clear hopping transport, and sample N5 is a marginal insulator; none of the insulating films show activated behavior characteristic of the insulating state adjacent to superconductivity in e.g. InO_x ^{26,48}.

Less disordered films (N0–N4) with lower nitrogen content x (or increased thickness) show quantum corrected metallic behavior below 20 K , with temperature-dependent conductivity contributions $\Delta\sigma(T) \sim \frac{e^2}{\pi h} \ln(T)$ from weak antilocalization and disorder-enhanced coulomb interactions in the normal state. Similar $\ln(T)$ temperature dependence is also observed in the normal state dependence of $\rho_{xy}(T)$. The lower panel of Fig. 4 highlights the superconducting transition at T_c for the samples shown, which ranges from $T_{c0} \sim 6.35 \text{ K}$ (sample N0) to 0.5 K (sample N4). With increasing disorder, the T_c of samples N1–N4 is suppressed; this can be attributed to the effect of enhanced coulomb interactions⁴⁹, as demonstrated in $\text{MoGe}^{50,51}$. The increase in disorder arises both from reducing film thickness (samples N0, N1, and N2) as well as increasing nitrogen composition x between samples N2, N4, and (insulating) N5. Resistive transitions are broadened due to enhanced superconducting fluctuation conductivity above T_c ³⁴. Below T_c , superconducting films all show a ‘foot’ arising from a cutoff in the diverging correlation length ξ due to film inhomogeneity⁵² or finite magnetic field⁵³; further details of the superconducting properties of these films can be found in Ref. 49.

V. FIELD-TUNED SIT

Superconductivity can be suppressed with application of critical fields $\mu_0 H_{c2} \approx 1 - 5 \text{ T}$, revealing an insulating normal state as $T \rightarrow 0$. Figure 5A (B) shows magnetoresistance isotherms for sample N3 (N4) at temperatures near $T_c = 0.5 \text{ K}$ (0.7 K); the approximate value for H_c

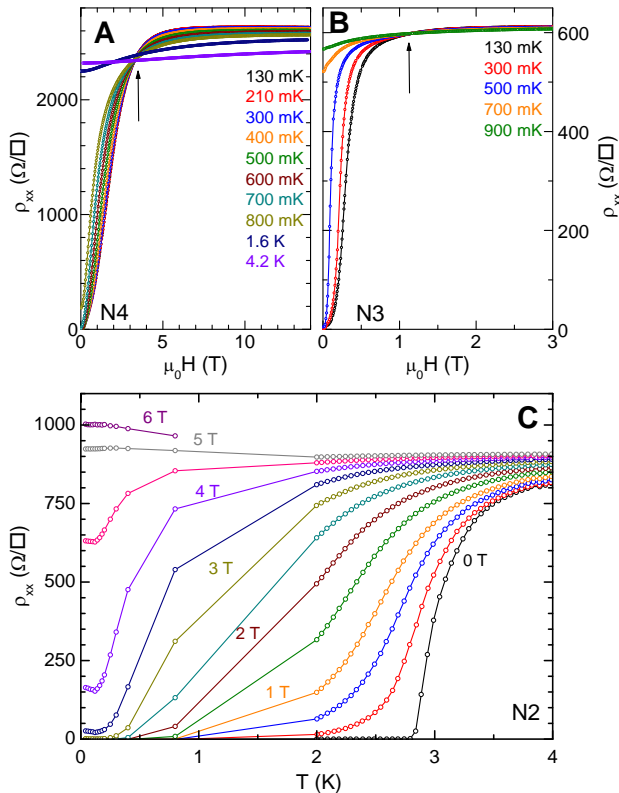


FIG. 5. (A-B) Magnetic field-tuned SIT in disordered a -Ta N_x films, evidenced by magnetoresistance isotherms for films N4 and N3. (C) Sheet resistance is plotted as a function of temperature for magnetic fields between 0 and 6 T as indicated, in equal steps. Lines are guides to the eye.

is indicated with an arrow. For $H < H_c$ the sample is superconducting; ρ_{xx} decreases with decreasing temperature. At high magnetic fields ρ_{xx} shows insulating behavior, diverging as $T \rightarrow 0$.

The field-tuned transition between superconducting and insulating temperature dependence is shown for sample N2 in Fig. 5C, which plots ρ_{xx} versus T curves in zero field and in applied fields of up to 6 T. The low-field curves show superconducting behavior with the value of T_c gradually suppressed with increasing magnetic field, the 6 T trace shows a negative slope $d\rho/dT$ to the lowest temperature available, ~ 100 mK, with $\rho_{xx} \sim \ln(T)$ again as expected for a quantum-corrected diffusive system. This insulating behavior persists unchanged with increasing magnetic fields.

At H_c there exists a temperature-independent crossing point, whose appearance is a hallmark for the SIT. In the “dirty boson” scenario for the SIT, the behavior near this quantum phase transition is described by the localization of Cooper pairs (or proliferation of vortices) in the presence of disorder at H_c . Tuning via magnetic field across the putative quantum critical point at H_c allows to investigate the critical scaling behavior in its vicinity.

VI. SCALING NEAR THE SIT

Having identified an apparent SIT in films where disorder has already suppressed T_c below the bulk value T_{c0} , we investigate the critical scaling behavior in the vicinity of the critical field H_c .^{54,55} Approaching the field-tuned transition (b-SIT) there is a diverging correlation length $\xi \sim (H - H_c)^{-\nu}$ with critical exponent ν . Nonzero temperatures cut off the vanishing frequency scale $\Omega \propto \xi^{-z}$, creating an additional length scale $L_{th} = (\hbar/k_B T)^{1/z}$ (here z is the dynamic critical exponent). Observables such as ρ_{xx} or ρ_{xy} must (in 2D) be a universal function \tilde{f} of the ratio ξ/L_{th} , through

$$\rho_{xx}(H, T) = \rho_c \tilde{f} \left(\frac{H - H_c}{T^{1/z\nu}} \right) \quad (2)$$

where ρ_c is the critical resistance at the transition, predicted in the dirty boson scenario to be $\rho_c = \rho_Q \equiv \frac{h}{4e^2}$. Thus isotherms of ρ_{xx} or ρ_{xy} should collapse above and below the b-SIT when plotted versus the scaling parameter $\eta \equiv \frac{H - H_c}{T^{1/z\nu}}$. The best collapse determines the product $z\nu$.

Figure 6 illustrates such finite-size scaling for three a -Ta N_x films, N2-N4. At left the raw magnetoresistance isotherms (in steps in temperature as indicated) cross at a common critical resistance ρ_c , with values ranging from 0.6-2.3 k Ω , all well below ρ_Q . At right in Fig. 6 are the same data versus the scaling parameter η . All three samples exhibit excellent scaling near H_c over a range of temperatures (for sample N2) well below T_c , and for samples N3 and N4 approximately up to T_c , with values of $z\nu \approx 1.25$. The scaling is disrupted at the lowest temperatures; such behavior has been seen previously in e.g. MoGe³ and InO_x.⁴⁸ We also note that values for H_c are comparable to H_{c2} estimated for each of these samples (collected in Table II). As discussed further below, these results are consistent with the “weak insulating” behavior seen in previous studies across a range of materials (and a range of disorder strengths)⁹. In none of these studies, however, has similar scaling behavior been resolved in the Hall resistance ρ_{xy} ; we consider such data in the next section.

TABLE II. Critical a -Ta N_x film parameters at the SIT. ρ_{xx}^{ns} is the resistance in the normal state, T_c is the transition temperature, ρ_c and H_c are the critical resistance and field at the transition, H_{c2} is an estimate for the mean-field upper critical field, and z and ν are critical exponents.

Sample	ρ_{xx}^n (k Ω)	T_c (K)	ρ_c (k Ω)	$\mu_0 H_c$ (T)	$\mu_0 H_{c2}(0)$ (T)	$z\nu$
N2	0.950	2.75	0.880	4.93	5.0	1.45 ± 0.1
N3	0.58	0.5	0.605	1.13	1.2	1.15 ± 0.1
N4	2.4	0.7	2.30	3.17	3.5	1.3 ± 0.1

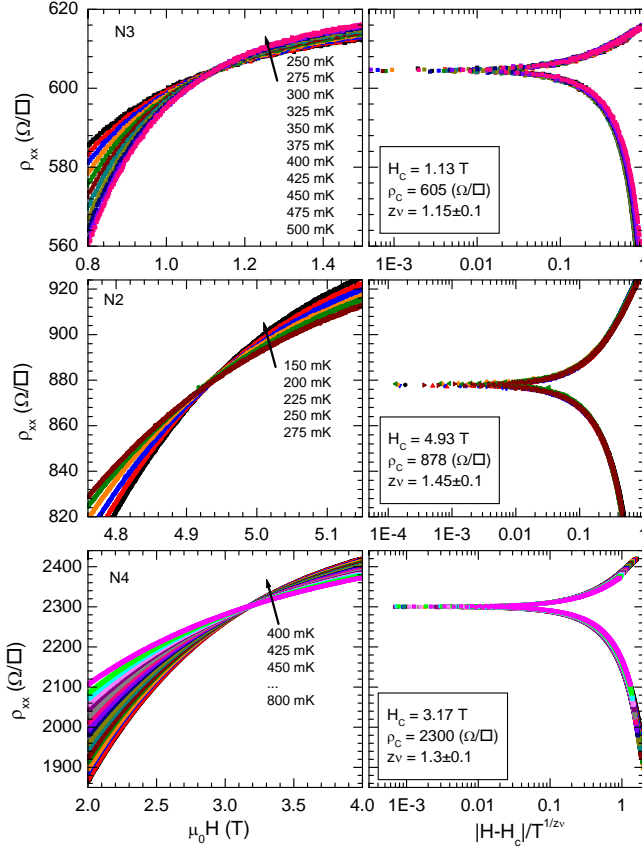


FIG. 6. Left panels: magnetoresistance isotherms for samples N3, N2, and N4 near the b-SIT. Right panels: resistance versus the scaling variable η for the identical datasets plotted at left, showing excellent collapse for a range of temperatures; collected scaling parameters are shown.

VII. HALL EFFECT

Early studies by Paalanen et al.³³ found a crossing point in ρ_{xy} in strongly disordered InO_x films beyond H_c , hypothesizing that this reflected the disappearance of the bosonic insulating behavior. Initial theoretical description of the dirty bosons scenario predicted scaling in ρ_{xy} in analogy with ρ_{xx} , with a universal value for ρ_{xy}^c :

$$\rho_{xy}(H, T) = \rho_{xy}^c \tilde{F}\left(\frac{H - H_c}{T^{1/z_v}}\right). \quad (3)$$

here again \tilde{F} is universal function, and ρ_{xy}^c was predicted to have a universal value. Subsequent analyses suggested that, due to “hidden” particle-hole symmetry, ρ_{xy}^c should vanish at the transition⁵⁶; despite ongoing debate as to the nature of the SIT, there have been no further systematic studies of ρ_{xy} in its vicinity. This is in part due to the challenge of measuring ρ_{xy} in materials where high carrier densities n lead to small signal sizes.

Early scaling theory⁵⁴ also predicted that (in the case of a self-dual transition) the value of ρ_{xy}^c would, together with the critical longitudinal resistance ρ_c , be given by

$$(\rho_{xy}^c)^2 + \rho_c^2 = \rho_Q^2. \quad (4)$$

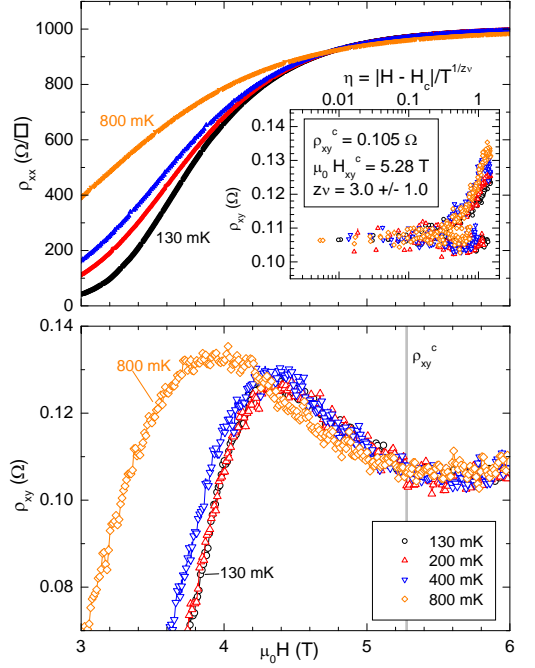


FIG. 7. Sheet resistance ρ_{xx} (upper panel) and Hall resistance ρ_{xy} (lower panel) versus magnetic field for TaN_x film N2. The magnetoresistance isotherms show a crossing point indicative of a field-tuned SIT; a similar crossing point can be seen in ρ_{xy} (lower panel). The Hall resistance shows weak scaling in the vicinity of the crossing point ρ_{xy}^c (gray bar), shown in the inset. Lines are guides to the eye.

Given that ρ_{xy} is typically much less than ρ_Q for non-insulating films, this would lead to the strong prediction of $\rho_c = \rho_Q$ that has been seen in many, but certainly not all, materials. However, in the weakly disordered $a\text{-TaN}_x$ films considered here, with large n , $R_H \ll 1 \Omega/\text{T}$, and thus $\rho_{xy} \ll 1 \Omega$, Eq. 4 would suggest that $\rho_c \approx \rho_Q$. But as seen in the previous section, $\rho_c \ll \rho_Q$ for all films at the field-tuned SIT, demonstrating that the non-universal ρ_c in $a\text{-TaN}_x$ cannot be explained by Eq. 4. Alternatively, a non-universal critical Hall resistance may be estimated as $\rho_{xy}^c = \rho_c \tan(\theta_H)$, where θ_H is the normal-state Hall angle.

Figure 7 shows ρ_{xy} across the field-tuned SIT in film N2 (lower panel), along with simultaneously measured ρ_{xx} (upper panel). The scale for ρ_{xy} has been enlarged to highlight the faint crossing in ρ_{xy} traces at 6.1 T; this is above $\mu_0 H_c \approx 4.9 \text{ T}$ found in the previous section. The normal state Hall angle for sample N2 is $\tan(\theta_H) = 7 \times 10^{-5}$ at 4.9 T, so $\rho_c \tan(\theta_H) \approx 0.07$, below but comparable to $\rho_{xy}^c = 0.105$. Following Eq. 3 we plot the scaled ρ_{xy} in the inset of Fig. 7. Apparently (as with ρ_{xx}) the critical Hall resistance ρ_{xy}^c is not universal; it is well below ρ_Q and the prediction $\rho_{xy}^c = 0.99 \times \rho_Q$ of Eq. 4.

VIII. DISCUSSION AND SUMMARY

Having identified both disorder- and field-tuned SIT in a -TaN_{*x*}, we can immediately address several of the key open questions surrounding this field. First, the critical disorder for the disorder suppression of superconductivity appears to be coincident with the disorder-driven (Anderson) metal-insulator transition. These TaN_{*x*} films show a metal-insulator transition as a function concentration x , with a critical value $x_c \sim 1.7$ and a critical resistivity comparable to that observed here⁴⁴. This coincidence is seen in NbSi²⁹ and NbN²⁸, and indicates for the SIT observed in these systems, a direct link between the appearance of (Fermionic) Anderson localization in the normal state, and the SIT.

Second, the superconductor-weak insulator transition (SWIT) observed in a -TaN_{*x*} appears to be a universal phenomenon. Although the appearance of a true $T = 0$ quantum phase transition is obscured by the poor scaling and unconventional metallic phase, an increasing number of materials show this phenomenology including MoGe, Ta, some InO_{*x*} films, and others. In particular critical scaling (with $z\nu \sim 1.25 \pm 0.25$) is comparable to the critical exponent for classical percolation $z\nu = 4/3$, $H_c \sim H_{c2}(0)$, and $\rho_c \ll \rho_Q$ ⁹. The presence of metallic ($n > 10^{22}\text{cm}^{-3}$) carrier densities appears to separate these materials from films of InO_{*x*} that show Bose-insulator behavior. Progress towards a coherent theoretical picture for the dissipative state²¹ will need to take this strong sensitivity to n into account.

Third, we have found evidence for critical scaling in another observable that is complementary to ρ_{xx} . Here ρ_{xy} appears to show a temperature-independent crossing point in both InO_{*x*} and in a -TaN_{*x*}; additional study is required to improve the quantitative analysis of the scaling

in ρ_{xy} , but its value at the transition ρ_{xy}^c is non-universal. This contrasts with the apparent universality of ρ_c ρ_Q in the strong disorder limit.

And finally, disorder in these “SWIT” materials cannot be linked to any macroscopic granularity or inhomogeneity. Thorough investigation of the a -TaN_{*x*} films showed no sign of any length scale for granular behavior in the composition or film structure; local spectroscopic probes may be necessary to study inhomogeneity length scales in the zero-temperatures phases near the SIT.

In summary, we have identified several features of the SIT in a new materials system, a -TaN_{*x*}. Tuning the nitrogen content gradually suppresses superconductivity and drives a disorder-tuned SIT. Weakly insulating films with disorder-suppressed T_c can be tuned via magnetic field through the SIT, and show signatures of the critical behavior arising from an underlying quantum critical point. Films with varying degrees of disorder show scaling consistent with classical percolation, with scaling disrupted at intermediate fields as $T \rightarrow 0$. Both ρ_{xx} and ρ_{xy} show non-universal critical resistances at the SIT, and the Hall effect shows weak scaling at a critical field close to H_c . Thus, a -TaN_{*x*} appears to represent a broad class of materials that show rich physics adjacent to the SIT that is distinct from the “classical” picture of disordered bosons.

ACKNOWLEDGMENTS

We thank the staff of the Stanford Nanocharacterization Laboratory for exhaustive characterization assistance. Initial work was supported by the National Science Foundation grant NSF-DMR-9508419. This work was supported by the Department of Energy Grant DE-AC02-76SF00515.

* Present address: Department of Physics, University of California, Berkeley, Berkeley, CA

¹ Allen M. Goldman and Nina Markovic. Superconductor-insulator transitions in the two-dimensional limit. *Physics Today*, 51(11):39–44, 1998.

² Vladimir Dobrosavljevic, Nandini Trivedi, and James M. Valles Jr. *Conductor Insulator Quantum Phase Transitions*. Oxford University Press, Oxford, UK, 2012. Subir Sachdev. *Quantum Phase Transitions, 2nd Ed*. Cambridge University Press, Cambridge, UK, 2011.

³ N. Mason and A. Kapitulnik. Dissipation effects on the superconductor-insulator transition in 2D superconductors. *Phys. Rev. Lett.*, 82:5341–5344, Jun 1999.

⁴ V. Yu. Butko and P. W. Adams. Quantum metallicity in a two-dimensional insulator. *Nature*, 409(6817):161, 2001.

⁵ T. I. Baturina, C. Strunk, M. R. Baklanov, and A. Satta. Quantum metallicity on the high-field side of the superconductor-insulator transition. *Phys. Rev. Lett.*, 98:127003, Mar 2007.

⁶ E. Abrahams, P. W. Anderson, D. C. Licciardello, and T. V. Ramakrishnan. Scaling theory of localization: absence of quantum diffusion in two dimensions. *Phys. Rev. Lett.*, 42:673–676, Dec 1979.

⁷ M. D. Stewart, Aijun Yin, J. M. Xu, and James M. Valles. Superconducting pair correlations in an amorphous insulating nanohoneycomb film. *Science*, 318(5854):1273–1275, 2007.

⁸ H. Q. Nguyen, S. M. Hollen, M. D. Stewart, J. Shainline, Aijun Yin, J. M. Xu, and J. M. Valles. Observation of giant positive magnetoresistance in a cooper pair insulator. *Phys. Rev. Lett.*, 103:157001, Oct 2009.

⁹ Myles A. Steiner, Nicholas P. Breznay, and Aharon Kapitulnik. Approach to a superconductor-to-bose-insulator transition in disordered films. *Phys. Rev. B*, 77:212501, Jun 2008.

¹⁰ Maoz Ovadia, David Kalok, Benjamin Sacepe, and Dan Shahar. Duality symmetry and its breakdown in the vicinity of the superconductor-insulator transition. *Nat. Phys.*, 9:415 – 418, 2013.

- ¹¹ Nicholas P. Breznay, Myles A. Steiner, Steven Allan Kivelson, and Aharon Kapitulnik. Self-duality and a hall-insulator phase near the superconductor-to-insulator transition in indium-oxide films. *Proceedings of the National Academy of Sciences*, 113(2):280–285, 2016.
- ¹² Ali Yazdani and Aharon Kapitulnik. Superconducting-insulating transition in two-dimensional *a*-MoGe thin films. *Phys. Rev. Lett.*, 74:3037–3040, Apr 1995.
- ¹³ D. Ephron, A. Yazdani, A. Kapitulnik, and M. R. Beasley. Observation of quantum dissipation in the vortex state of a highly disordered superconducting thin film. *Phys. Rev. Lett.*, 76:1529–1532, Feb 1996.
- ¹⁴ Yongguang Qin, Carlos L. Vicente, and Jongsoo Yoon. Magnetically induced metallic phase in superconducting tantalum films. *Phys. Rev. B*, 73:100505, Mar 2006.
- ¹⁵ Yu Saito, Yuichi Kasahara, Jianting Ye, Yoshihiro Iwasa, and Tsutomu Nojima. Metallic ground state in an ion-gated two-dimensional superconductor. *Science*, 350(6259):409–413, 2015.
- ¹⁶ A. W. Tsen, B. Hunt, Y. D. Kim, Z. J. Yuan, S. Jia, R. J. Cava, J. Hone, P. Kim, C. R. Dean, and A. N. Pasupathy. Nature of the quantum metal in a two-dimensional crystalline superconductor. *Nat Phys*, 12:208–212, 2016.
- ¹⁷ Efrat Shimshoni, Assa Auerbach, and Aharon Kapitulnik. Transport through quantum melts. *Phys. Rev. Lett.*, 80:3352–3355, Apr 1998.
- ¹⁸ Aharon Kapitulnik, Nadya Mason, Steven A. Kivelson, and Sudip Chakravarty. Effects of dissipation on quantum phase transitions. *Phys. Rev. B*, 63:125322, Mar 2001.
- ¹⁹ B. Spivak, A. Zyuzin, and M. Hruska. Quantum superconductor-metal transition. *Phys. Rev. B*, 64:132502, Aug 2001.
- ²⁰ Michael Mulligan and S. Raghu. Composite fermions and the field-tuned superconductor-insulator transition. *Phys. Rev. B*, 93:205116, May 2016.
- ²¹ Richard A. Davison, Luca V. Delacrétaz, Blaise Goutéraux, and Sean A. Hartnoll. Hydrodynamic theory of quantum fluctuating superconductivity. *Phys. Rev. B*, 94:054502, Aug 2016.
- ²² N. P. Breznay and A. Kapitulnik. *unpublished*, 2017.
- ²³ C. A. Marrache-Kikuchi, H. Aubin, A. Pourret, K. Behnia, J. Lesueur, L. Bergé, and L. Dumoulin. Thickness-tuned superconductor-insulator transitions under magnetic field in *a*-nbsi. *Phys. Rev. B*, 78:144520, Oct 2008.
- ²⁴ T. I. Baturina, D. R. Islamov, J. Bentner, C. Strunk, M. R. Baklanov, and A. Satta. Superconductivity on the localization threshold and magnetic-field-tuned superconductor-insulator transition in tin films. *Journal of Experimental and Theoretical Physics Letters*, 79(7):337–341, 2004.
- ²⁵ Mintu Mondal, Anand Kamlapure, Madhavi Chand, Garima Saraswat, Sanjeev Kumar, John Jesudasan, L. Benfatto, Vikram Tripathi, and Pratap Raychaudhuri. Phase fluctuations in a strongly disordered *s*-wave nbn superconductor close to the metal-insulator transition. *Phys. Rev. Lett.*, 106:047001, Jan 2011.
- ²⁶ G. Sambandamurthy, L. W. Engel, A. Johansson, and D. Shahar. Superconductivity-related insulating behavior. *Phys. Rev. Lett.*, 92:107005, Mar 2004.
- ²⁷ T. I. Baturina, A. Yu. Mironov, V. M. Vinokur, M. R. Baklanov, and C. Strunk. Localized superconductivity in the quantum-critical region of the disorder-driven superconductor-insulator transition in tin thin films. *Phys. Rev. Lett.*, 99:257003, Dec 2007.
- ²⁸ Madhavi Chand, Garima Saraswat, Anand Kamlapure, Mintu Mondal, Sanjeev Kumar, John Jesudasan, Vivas Bagwe, Lara Benfatto, Vikram Tripathi, and Pratap Raychaudhuri. Phase diagram of the strongly disordered *s*-wave superconductor nbn close to the metal-insulator transition. *Phys. Rev. B*, 85:014508, Jan 2012.
- ²⁹ O. Crauste, F. Couëdo, L. Bergé, C. A. Marrache-Kikuchi, and L. Dumoulin. Destruction of superconductivity in disordered materials: A dimensional crossover. *Phys. Rev. B*, 90:060203, Aug 2014.
- ³⁰ Y. Seo, Y. Qin, C. L. Vicente, K. S. Choi, and Jongsoo Yoon. Origin of nonlinear transport across the magnetically induced superconductor-metal-insulator transition in two dimensions. *Phys. Rev. Lett.*, 97:057005, Aug 2006.
- ³¹ Yize Li, Carlos L. Vicente, and Jongsoo Yoon. Transport phase diagram for superconducting thin films of tantalum with homogeneous disorder. *Phys. Rev. B*, 81:020505, Jan 2010.
- ³² Sungyu Park, Junghyun Shin, and Eunseong Kim. Scaling analysis of field-tuned superconductorinsulator transition in two-dimensional tantalum thin films. *Scientific Reports*, 7:42969, 2017.
- ³³ M. A. Paalanen, A. F. Hebard, and R. R. Ruel. Low-temperature insulating phases of uniformly disordered two-dimensional superconductors. *Phys. Rev. Lett.*, 69:1604–1607, Sep 1992.
- ³⁴ Nicholas P. Breznay, Karen Michaeli, Konstantin S. Tikhonov, Alexander M. Finkel’stein, Mihir Tendulkar, and Aharon Kapitulnik. Hall conductivity dominated by fluctuations near the superconducting transition in disordered thin films. *Phys. Rev. B*, 86:014514, Jul 2012.
- ³⁵ Nicholas P. Breznay and Aharon Kapitulnik. Observation of the ghost critical field for superconducting fluctuations in a disordered tan thin film. *Phys. Rev. B*, 88:104510, Sep 2013.
- ³⁶ H.B. Nie, S.Y. Xu, S.J. Wang, L.P. You, Z. Yang, C.K. Ong, J. Li, and T.Y.F. Liew. Structural and electrical properties of tantalum nitride thin films fabricated by using reactive radio-frequency magnetron sputtering. *Applied Physics A*, 73(2):229–236, 2001.
- ³⁷ C.-S. Shin, Y.-W. Kim, D. Gall, J.E. Greene, and I. Petrov. Phase composition and microstructure of polycrystalline and epitaxial TaN_x layers grown on oxidized Si(001) and MgO(001) by reactive magnetron sputter deposition. *Thin Solid Films*, 402(12):172 – 182, 2002.
- ³⁸ Suguru Noda, Kun Tepsanongsuk, Yoshiko Tsuji, Yuya Kajikawa, Yoshifumi Ogawa, and Hiroshi Komiyama. Preferred orientation and film structure of TaN films deposited by reactive magnetron sputtering. *Journal of Vacuum Science & Technology A: Vacuum, Surfaces, and Films*, 22(2):332–338, 2004.
- ³⁹ Katsuhiko Wakasugi, Mie Tokunaga, Taishi Sumita, Hiroshi Kubota, Masanori Nagata, and Yukio Honda. Superconductivity of reactivity sputtered TaN film for ULSI process. *Physica B: Condensed Matter*, 239(12):29 – 31, 1997. Proceedings of the Workshop on Transition Metals and Compounds under Multiextreme Conditions.
- ⁴⁰ F. M. Kilbane and P. S. Habig. Superconducting transition temperatures of reactively sputtered films of tantalum nitride and tungsten nitride. *Journal of Vacuum Science and Technology*, 12(1):107–109, 1975.
- ⁴¹ V. G. Prokhorov. Dependence of the superconducting transition temperature on the thickness of superconducting films with different coherence lengths. *Low Temperature*

- Physics*, 24(6):410–413, 1998.
- ⁴² C.-S. Shin, D. Gall, Y.-W. Kim, P. Desjardins, I. Petrov, J. E. Greene, M. Oden, and L. Hultman. Epitaxial NaCl structure δ -TaN_x(001): Electronic transport properties, elastic modulus, and hardness versus N/Ta ratio. *Journal of Applied Physics*, 90(6):2879–2885, 2001.
 - ⁴³ T. Riekkinen and J. Molarius. Reactively sputtered tantalum pentoxide thin films for integrated capacitors. *Micro-electronic Engineering*, 70(24):392 – 397, 2003. Materials for Advanced Metallization 2003.
 - ⁴⁴ L. Yu, C. Stampfl, D. Marshall, T. Eshrich, V. Narayanan, J. M. Rowell, N. Newman, and A. J. Freeman. Mechanism and control of the metal-to-insulator transition in rocksalt tantalum nitride. *Phys. Rev. B*, 65:245110, Jun 2002.
 - ⁴⁵ D. B. Haviland, Y. Liu, and A. M. Goldman. Onset of superconductivity in the two-dimensional limit. *Phys. Rev. Lett.*, 62:2180–2183, May 1989.
 - ⁴⁶ A L Efros and B I Shklovskii. Coulomb gap and low temperature conductivity of disordered systems. *Journal of Physics C: Solid State Physics*, 8(4):L49, 1975.
 - ⁴⁷ Ralph Rosenbaum. Crossover from mott to Efros-Shklovskii variable-range-hopping conductivity in In_xO_y films. *Phys. Rev. B*, 44:3599–3603, Aug 1991.
 - ⁴⁸ Myles Steiner and Aharon Kapitulnik. Superconductivity in the insulating phase above the field-tuned superconductor-insulator transition in disordered indium oxide films. *Physica C: Superconductivity*, 422(1-2):16 – 26, 2005.
 - ⁴⁹ N. P. Breznay. PhD thesis, Stanford University, 2013.
 - ⁵⁰ A. M. Finkelshtein. Superconducting transition temperature in amorphous films. *JETP Lett.*, 45:46, 1987.
 - ⁵¹ J. M. Graybeal and M. R. Beasley. Localization and interaction effects in ultrathin amorphous superconducting films. *Phys. Rev. B*, 29:4167–4169, Apr 1984.
 - ⁵² L. Benfatto, C. Castellani, and T. Giamarchi. Broadening of the berezinskii-kosterlitz-thouless superconducting transition by inhomogeneity and finite-size effects. *Phys. Rev. B*, 80:214506, Dec 2009.
 - ⁵³ J. W. P. Hsu and A. Kapitulnik. Superconducting transition, fluctuation, and vortex motion in a two-dimensional single-crystal Nb film. *Phys. Rev. B*, 45:4819–4835, Mar 1992.
 - ⁵⁴ Matthew P. A. Fisher. Quantum phase transitions in disordered two-dimensional superconductors. *Phys. Rev. Lett.*, 65:923–926, Aug 1990.
 - ⁵⁵ Matthew P. A. Fisher, G. Grinstein, and S. M. Girvin. Presence of quantum diffusion in two dimensions: Universal resistance at the superconductor-insulator transition. *Phys. Rev. Lett.*, 64:587–590, Jan 1990.
 - ⁵⁶ Matthew P.A. Fisher. Hall effect at the magnetic-field-tuned superconductor-insulator transition. *Physica A: Statistical Mechanics and its Applications*, 177(13):553 – 560, 1991.